Electrochemistry Communications 114 (2020) 106701

Contents lists available at ScienceDirect

Electrochemistry Communications

journal homepage: www.elsevier.com/locate/elecom

A one-step method to prepare analogue of NiC_x for electrochemical water splitting

Shan Zhang[a,b], Xiaoyan Zhang[a], Haishuang Zhu[a,b], Huanhuan Xing[a,b], Jing Li[a,b,*], Erkang Wang[a,b,*]

[a] State Key Laboratory of Electroanalytical Chemistry, Changchun Institute of Applied Chemistry, Chinese Academy of Sciences, Changchun, Jilin 130022, China
[b] University of Science and Technology of China, Hefei, Anhui 230029, China

ARTICLE INFO

Keywords:
One-step method
Analogue of NiC_x
Water splitting
Excellent activity

ABSTRACT

The development of high-activity and low-cost electrocatalysts through simple one-step method is of vital importance for electrocatalytic water splitting, but still remains a challenge. In this work, ternary Ni-N-P microparticles, an analogue of NiC_x, are *in-situ* grown on nickel foam through one-step phosphorization at low temperature under atmosphere of ammonia. The unique microparticles-like morphology and suitable electronic structure render them enhanced electron and mass transfer ability, ensuring superior activity and good durability in catalyzing oxygen evolution reaction (OER) and hydrogen evolution reaction (HER) under alkaline condition. Specifically, the optimal Ni-N-P microparticles can deliver 10 mA/cm^2 at the overpotential of 260 mV and 180 mV *vs.* reversible hydrogen electrode (RHE) for OER and HER, respectively. Additionally, only a cell voltage of 1.7 V is required to afford 10 mA/cm^2 when the prepared Ni-N-P microparticles serve as both anode and cathode in two-electrode configuration for overall water splitting. The Ni-N-P microparticles hold promise as cost-effective and efficient candidate for practical water splitting devices.

1. Introduction

Electrochemical water splitting is an attractive approach to not only provide high-purity chemical raw material (H_2), but also store intermittent sources such as sunlight and wind in the form of chemical energy [1]. Currently, its large-scale application is greatly hampered by the lack of active and low-cost electrocatalysts to expedite the reaction process, including the anodic OER and HER at the cathode [2,3]. Therefore, efficient catalysts are highly required to accelerate sluggish dynamics and reduce the needed overpotential. Despite favorable kinetics on Pt-based metals for HER [4] and Ru/Ir-based materials for OER [5], they suffer from rare reserves and high cost [6], which largely hinder their wide-range practical application. Developing non-noble materials with high activity for both OER and HER is accordingly imperative and desirable.

Inspired by the partially filled 3d-orbital and earth-abundant nature, the first-raw transition-metal compounds, especially nickel-based materials, have emerged as an alternative and effective water splitting catalysts [7]. Much efforts has been dedicated to explore various compositions and structures of nickel-based compounds, including nickel sulfides [8,9], phosphides [10,11], (hydro)oxides [12,13] and nitrides [14,15]. Given the intrinsically metallic properties and excellent electronic conductivity, Ni_3N receives special attention and shows great potential as effective OER/HER electrocatalysts [16]. In general, there are two steps to prepare Ni_3N, the first one is to synthesize Ni precursors such as NiO and $Ni(OH)_2$, then reacted with N sources such as azides and ammonia (NH_3) [17–19]. Although this method is well-developed, high temperature ($\geq$400 °C) or long reaction time ($\geq$5h) are usually required [14,20–22]. In contrast, developing facile one-step method through reaction between existing Ni and N source, for example N_2 plasma activated nickel foam (NF) [23], is much more competitive. As a 3D porous substrate, the usage of NF can provide Ni source, increase the surface area and avoid using the polymer binder. However, studies that involve NF as Ni source directly are still very limited [24,25] and exploring simple one-step calcination approach to prepare NF-based compounds as effective catalysts for water splitting needs further investigation.

Herein, ternary compound of Ni-N-P microparticles were in-situ grown on NF by one-step phosphorization at low temperature of 300 °C under the atmosphere of NH_3, which applied $NaH_2PO_2{\cdot}H_2O$ and NH_3 as

* Corresponding author at: State Key Laboratory of Electroanalytical Chemistry, Changchun Institute of Applied Chemistry, Chinese Academy of Sciences, Changchun, Jilin 130022, China.
E-mail addresses: lijingce@ciac.ac.cn (J. Li), ekwang@ciac.ac.cn (E. Wang).

https://doi.org/10.1016/j.elecom.2020.106701
Received 17 December 2019; Received in revised form 16 February 2020; Accepted 20 February 2020
Available online 07 March 2020

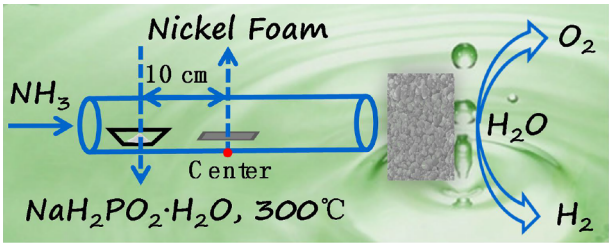

Scheme 1. Schematic diagram of preparation procedure and electrocatalytic application of the Ni-N-P microparticles.

P and N sources, respectively. Of note, the presence of $NaH_2PO_2{\cdot}H_2O$ is essential for the reaction between NF and NH_3 in such low temperature and short reaction time. Due to the increased surface area and tailored electronic structure that benefit reaction process, the obtained Ni-N-P microparticles exhibit excellent activity and robust stability towards OER/HER, which can afford the current density of 10 mA/cm^2 at the overpotential of 260 mV and 180 mV *vs.* RHE for OER and HER, respectively. Moreover, when assemble the Ni-N-P microparticles into water splitting device, it only needs a cell voltage of 1.7 V to deliver the current density of 10 mA/cm^2 with satisfactory long-time stability.

2. Experimental section

2.1. Reagents

$NaH_2PO_2{\cdot}H_2O$ was obtained from Sigma-Aldrich. Potassium hydroxide (KOH) was provided by Beijing Chemical Co., Ltd. (China). Water was purified through Millipore system.

2.2. Synthesis of Ni-N-P catalysts

To produce Ni-N-P catalysts, NF (2 cm × 3 cm) and 1 g $NaH_2PO_2{\cdot}H_2O$ were placed in two separate porcelain boats, then put the NF at the middle of the tube furnace and $NaH_2PO_2{\cdot}H_2O$ at the upstream 10 cm far from the NF. Afterward, the tube furnace was heated to 300 ℃ for 2 h with a ramp rate of 5 ℃/min, then cooled down naturally under the protection of NH_3.

As control experiments, Ni-N and Ni-P catalysts were also synthesized through similar procedure. Specifically, the NF was calcined at 300 ℃ for 2 h under the atmosphere of NH_3 without the $NaH_2PO_2{\cdot}H_2O$ to obtain the Ni-N catalysts. As for the preparation of the Ni-P catalysts, the NF went through phosphorization (300 ℃ for 2 h) with the presence of $NaH_2PO_2{\cdot}H_2O$ under the atmosphere of Ar.

2.3. Characterization

Scanning electron microscopy (SEM) and energy dispersive X-ray (EDX) measurements were collected using a PHILIPS XL-30 ESEM at an acceleration voltage of 20 kV. High-resolution transmission electron microscopy (HRTEM) was performed on JEM-2100F transmission electron microscope (200 kV). Powder X-ray diffraction (XRD) profiles were performed on a X'Pert-Pro MPD diffractometer. The X-ray photoelectron spectroscopy (XPS) spectra were recorded on ESCALAB-MKII 250 photoelectron spectrometer with Al Kα radiation.

2.4. Electrochemical measurements

The electrochemical tests were performed on CHI660E workstation (Shanghai, China). A graphite rod and the Ag/AgCl electrode were applied as counter and reference electrode, respectively. The Ag/AgCl electrode was calibrated to RHE: E (RHE) = E (Ag/AgCl) + 0.954 V (1 M KOH). Linear sweep voltammetry (LSV) measurements were carried out in O_2-saturated 1 M KOH for OER and N_2-saturated electrolyte for HER with a scan rate of 5 mV/s, respectively. For Tafel slope calculation, the scan rate was reduced to 1 mV/s. Electrochemical impedance spectroscopy (EIS) profile was recorded over a frequency range from 0.01 Hz to 10 KHz. To calculate the electrochemically active surface area (ECSA), cyclic voltammetry (CV) was conducted with potential range of 0.1 ~ 0.2 V (*vs.* RHE). The Chronoamperometric test of Ni-N-P microparticles for HER and OER was performed at the constant potential of −0.18 V and 1.52 V (*vs.* RHE). Assuming all Ni are active sites, the turn over frequency (TOF) for OER and HER was calculated by the equation [26]:

$$TOF = \frac{I}{n \times F \times m}$$

where I is the current (A); n is the stoichiometric number of consumed electrons (n = 2 and 4 for HER and OER, respectively); F is the Faraday

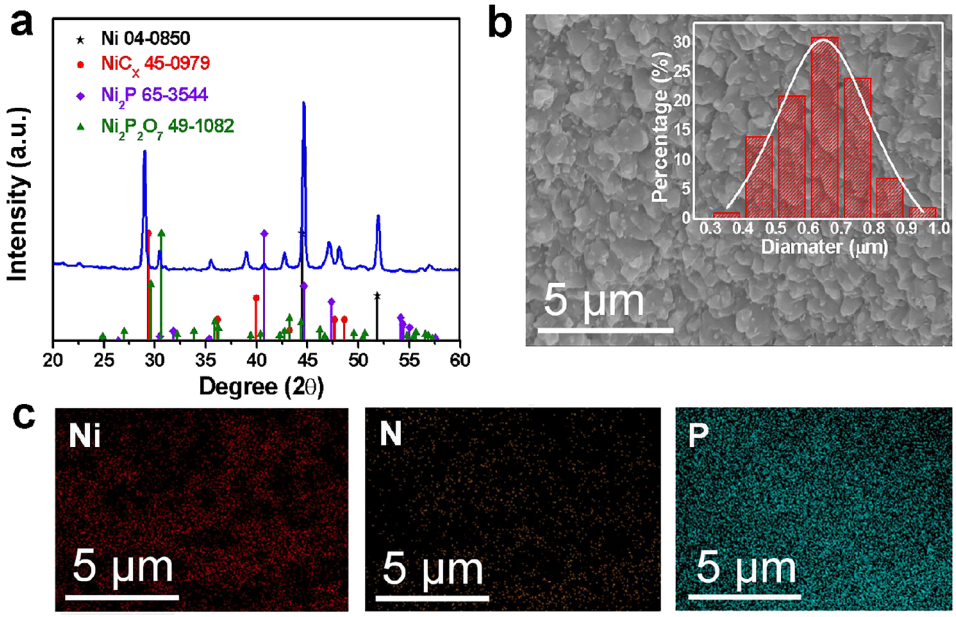

Fig. 1. (a) The XRD pattern of the obtained Ni-N-P microparticles. (b) SEM image and (c) the EDX-mapping of the resulted Ni-N-P microparticles. Inset in (b): size distribution of Ni-N-P microparticles.

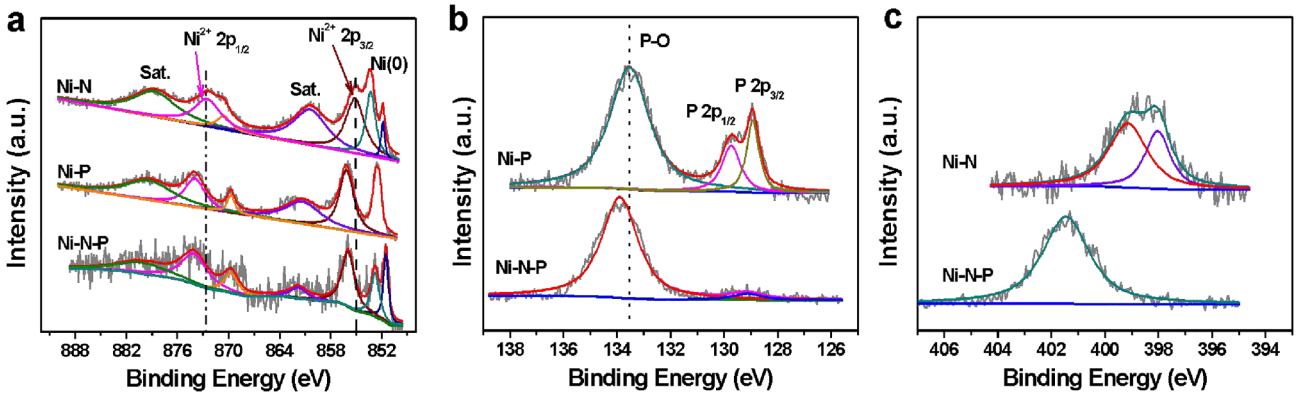

Fig. 2. XPS spectra for (a) Ni 2p, (b) P 2p and (c) N 1s of Ni-N, Ni-P and ternary Ni-N-P microparticles.

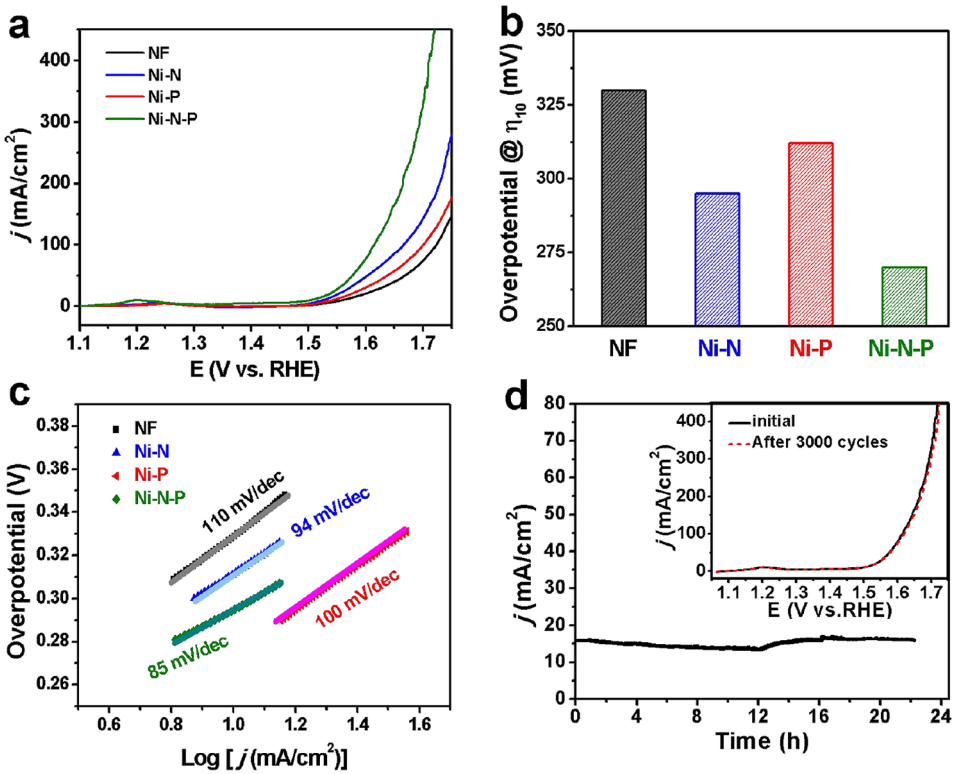

Fig. 3. (a) LSV curves of NF, Ni-N, Ni-P and Ni-N-P microparticles at scan rate of 5 mV/s. (b) The histogram of needed overpotential for various catalysts to drive the current density of 10 mA/cm^2. (c) The Tafel slopes. (d) Chronoamperometric curve of Ni-N-P microparticles for OER. Inset: Polarization curves of Ni-N-P microparticles before and after 3000 CV cycles.

constant (96485 C/mol) and m is the moles of active sites. All potential was versus RHE and all current was 80% *iR*-corrected.

3. Results and discussion

Facile low-temperature calcination method was applied to prepare ternary Ni-N-P microparticles using NF as Ni source, $NaH_2PO_2{\cdot}H_2O$, NH_3 as P and N sources, respectively (Scheme 1). The XRD pattern of Ni-N-P microparticles (Fig. 1a) shows several sharp peaks, implying the high crystallinity of the products. Interestingly, these peaks do not match that of any standard diffraction patterns for single nickel phosphides or nitrides, however, most peaks can be indexed to that of the NiC_x (JCPDS No. 45–0979). It has been reported that NiC_x is active for catalyzing OER process [27,28], the obtained Ni-N-P microparticles are accordingly expected to be an effective OER catalysts owing to the close resemblance in crystal phase. Of note, Small amount of phosphides existed and slight oxidation occurred on the surface due to the XRD pattern. The morphology of the ternary Ni-N-P compound is proved to be irregular microparticles with average size of 640 nm (Fig. 1b and inset). The corresponding EDX spectrum (Fig. 1c) confirm the homogeneous distribution of Ni, N and P elements, and the composition was collected in Table S1. The lattice spacing of 0.3 nm in the HRTEM image (Fig. S1) is consistent with the (1 1 1) plane of NiC_x. In addition, the products of Ni-N and Ni-P were also synthesized for better comparison. The Ni-P products displayed similar microparticles morphology to that of the ternary Ni-N-P (Fig. S2a and Fig. S2b). While the resulting Ni-N products (Fig. S2c and Fig. S2d) exhibited featureless morphology.

The chemical state of the products was identified by XPS. Fig. 2a shows the Ni 2p spectrum for Ni-N, Ni-P and Ni-N-P compounds. For Ni-N, two peaks centered at 856.2 eV and 873.9 eV belong to the Ni $2p_{3/2}$ and Ni $2p_{1/2}$ of Ni^{2+}, respectively, with bands of 861.3 eV and 879.3 eV appeared as the satellite peaks [29,30]. As for Ni-P and Ni-N-P, the binding energy of 852.5 eV and 869.9 eV can be assigned to the Ni-P species; while the peaks at 856.2 eV and 873.9 eV correspond to the Ni-O species due to the some oxidation by air [31,32]. Electronic interaction would be enhanced due to the stronger electronegativity of oxygen, which is beneficial for the OER process. The peak fitting result of P 2p for Ni-P (Fig. 2b) exhibits two different bindings, wherein the doublet at 128.9 eV and 129.7 eV is attributed to P-Ni binding [33]. The

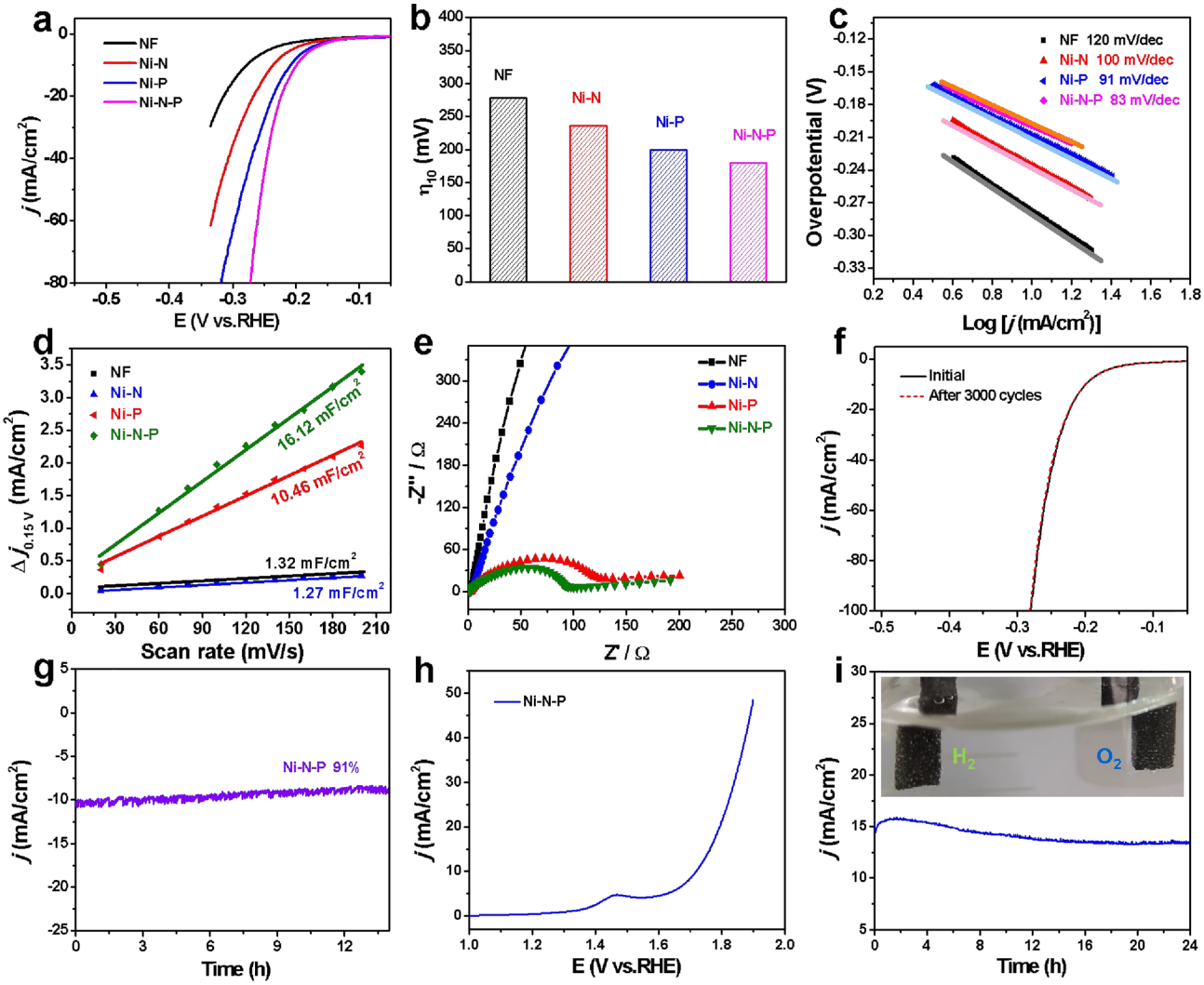

Fig. 4. (a) HER performance of NF, Ni-N, Ni-P and Ni-N-P at scan rate of 5 mV/s. (b) The histogram of overpotential at the current density of 10 mA/cm^2 for HER. (c) The Tafel slopes. (d) The Cdl and (e) EIS plots of various catalysts. (f) The HER performance of Ni-N-P before and after 3000 CV cycles. (g) Chronoamperometric curve of Ni-N-P for HER. (h) The LSV curve and (i) the chronopotentiometric curve of water electrolyzer. Inset in (i): the image of H_2 and O_2 bubbles released from the surface of ternary Ni-N-P microparticles.

peak of P-Ni binding almost vanishes completely after the introduction of N, suggesting the modulated electronic interaction between Ni, P and N. As for N 1s spectrum of Ni-N sample (Fig. 2c), it can be deconvoluted into two kinds of bindings, one is possible Ni-N binding of 398.03 eV, and the other (399.01 eV) is similar to that of pyridinic N [33]. However, only one peak (401.4 eV) that close to that of graphitic N is observed for Ni-N-P sample [34], which may imply the different structure of ternary Ni-N-P microparticles.

The OER performance of the obtained Ni-based catalysts was then evaluated. Fig. 3a displays the *iR*-corrected LSV curves. Apparently, the ternary Ni-N-P microparticles exhibit best performance with an overpotential of 260 mV *vs.* RHE at 10 mA/cm^2, exceeding those of Ni-N (295 mV *vs.* RHE), Ni-P (312 mV *vs.* RHE) and the substrate NF (330 mV *vs.* RHE, Fig. 3b). The Tafel slope for Ni-N-P microparticles is calculated to be 85 mV dec^{-1} (Fig. S3 and Fig. 3c), indicating the more favorable catalytic OER kinetics. For OER, the formation of absorbed OOH species is generally identified as rate-limiting step [35,36], so we suspect that the tailored electronic structure of ternary Ni-N-P microparticles lowers the energy barrier for the formation of OOH species, thus leading to the impovement of OER activity. To investigate the intrinsic activity of the product, the TOF for OER was determined as 0.003 s^{-1} (300 mV *vs.* RHE). Additionally, we evaluate the stability of ternary Ni-N-P microparticles by chronoamperometry measurement (Fig. 3d). The current density could maintain ~15 mA/cm^2 for almost 24 h. Also, the catalytic activity do not show any observable decay after 3000 CV cycles (inset in Fig. 3d), implying the outstanding stability of the ternary Ni-N-P microparticles for OER.

Besides the excellent OER performance, the prepared Ni-N-P microparticles also show apparent activity towards HER. As shown in Fig. 4a, the ternary Ni-N-P microparticles exhibit the highest HER activity. To deliver the current density of 10 mA/cm^2, the ternary Ni-N-P microparticles require an overpotential of 180 mV *vs.* RHE (Fig. 4b), which is much smaller than those of other samples. Linear fitting the Tafel data results in a Tafel slope of 83 mV dec^{-1} for ternary Ni-N-P microparticles (Fig. S4 and Fig. 4c), reflecting the HER pathway follows Volmer-Heyrovsky mechanism [37]. The TOF of ternary Ni-N-P microparticles for HER is 0.0002 s^{-1} (200 mV *vs.* RHE). To further explore the origin of enhanced HER activity, the ECSA was estimated by calculating the electrical double-layer capacitance (C_{dl}, Fig. S5) [38]. As expected, the Ni-N-P microparticles display highest C_{dl} value, more than ten times larger than that of Ni-N product (Fig. 4d). Meanwhile, EIS was conducted to gain insights into the charge transfer process (Fig. 4e). It can be easily observed that the ternary Ni-N-P microparticles possess smallest charge transfer resistance. Moreover, the

obtained Ni-N-P microparticles possess outstanding cycling stability with no obvious degradation after continuous 3000 CV cycles (Fig. 4f). And the rather good stability is also corroborated by the chronoamperometric measurement (Fig. 4g), which is able to preserve 91% of the current density after 12 h operation.

Encouraged by the good OER and HER performance, an electrolyzer is assembled for water splitting with ternary Ni-N-P microparticles served as both anode and cathode. Fig. 4h shows the polarization curve, which can afford a current density of 10 mA/cm^2 at the cell voltage of 1.7 V (Table S2). Further, the Ni-N-P microparticles electrodes demonstrate good long-time stability. The current density displays a slight attenuation and then levels off (Fig. 4i), with gas bubbles produce and release from the electrode surface continuously (inset in Fig. 4i), which illuminates its potential as efficient electrocatalysts for water splitting.

4. Conclusion

In summary, the ternary Ni-N-P microparticles that grown on NF are successfully prepared by facile one-step phosphorization, which serve as efficient electrocatalysts for overall water splitting. As water splitting electrolyzer, it only needs a cell voltage of 1.7 V to deliver the current density of 10 mA/cm^2 with robust long-time stability. The excellent performance can be attributed to the higher surface area and suitable electronic structure, thus leading to more accessible active sites and enhanced electron transport. Featured with low-cost, readily sc alable synthesis and high catalytic activity, our work offers a specific example to uncover the binder-free electrode with tunable compositions can be developed for efficient water electrolysis.

CRediT authorship contribution statement

Shan Zhang: Investigation, Data curation, Writing - original draft. **Xiaoyan Zhang:** Data curation, Validation. **Haishuang Zhu:** Data curation. **Huanhuan Xing:** Data curation. **Jing Li:** Writing - review & editing, Project administration. **Erkang Wang:** Supervision, Writing - review & editing, Project administration.

Declaration of Competing Interest

The authors declare that they have no known competing financial interests or personal relationships that could have appeared to influence the work reported in this paper.

Acknowledgments

This work was supported by National Natural Science Foundation of China (Grant No. 21427811 and 21721003), MOST, China (Grant No.2016YFA0203200), Youth Innovation Promotion Association CAS (Grant No. 2016208) and Jilin Province Science Technology Development Plan Project 20170101194JC.

References

[1] B.Q. Li, S.Y. Zhang, C. Tang, X. Cui, Q. Zhang, Anionic regulated NiFe (Oxy)sulfide electrocatalysts for water oxidation, Small 13 (2017) 1700610.
[2] Y. Wang, Y. Zhang, Z. Liu, C. Xie, S. Feng, D. Liu, M. Shao, S. Wang, Layered double hydroxide nanosheets with multiple vacancies obtained by dry exfoliation as highly efficient oxygen evolution electrocatalysts, Angew. Chem., Int. Ed. 56 (2017) 5867–5871.
[3] S. Anantharaj, S.R. Ede, K. Sakthikumar, K. Karthick, S. Mishra, S. Kundu, Recent trends and perspectives in electrochemical water splitting with an emphasis on sulfide, selenide, and phosphide catalysts of Fe Co, and Ni: a review, ACS Catal. 6 (2016) 8069–8097.
[4] W. Chen, J. Pei, C.T. He, J. Wan, H. Ren, Y. Zhu, Y. Wang, J. Dong, S. Tian, W.C. Cheong, S. Lu, L. Zheng, X. Zheng, W. Yan, Z. Zhuang, C. Chen, Q. Peng, D. Wang, Y. Li, Rational design of single molybdenum atoms anchored on N-doped carbon for effective hydrogen evolution reaction, Angew. Chem., Int. Ed. 56 (2017) 16086–16090.
[5] G. Li, S. Li, J. Ge, C. Liu, W. Xing, Discontinuously covered IrO_2–RuO_2@Ru electrocatalysts for the oxygen evolution reaction: how high activity and long-term durability can be simultaneously realized in the synergistic and hybrid nanostructure, J. Mater. Chem. A 5 (2017) 17221–17229.
[6] P.A. Huabin Zhang, Bu Wei Zhou, Yuan Guan, Peng Zhang, Juncai Dong, Xiong Wen (David) Lou, Dynamic traction of lattice-confined platinum atoms into mesoporous carbon matrix for hydrogen evolution reaction, Sci. Adv. 4 (2018) eaao6657.
[7] Z. Qiu, C.-W. Tai, G.A. Niklasson, T. Edvinsson, Direct observation of active catalyst surface phases and the effect of dynamic self-optimization in NiFe-layered double hydroxides for alkaline water splitting, Energy Environ. Sci. 12 (2019) 572–581.
[8] P. Luo, H. Zhang, L. Liu, Y. Zhang, J. Deng, C. Xu, N. Hu, Y. Wang, Targeted synthesis of unique nickel sulfide (NiS, NiS_2) microarchitectures and the applications for the enhanced water splitting system, ACS Appl. Mater. Interfaces 9 (2017) 2500–2508.
[9] B. You, Y. Sun, Hierarchically porous nickel sulfide multifunctional superstructures, Adv. Energy Mater. 6 (2016) 1502333.
[10] Y. Li, C. Zhao, Enhancing water oxidation catalysis on a synergistic phosphorylated NiFe hydroxide by adjusting catalyst wettability, ACS Catal. 7 (2017) 2535–2541.
[11] Y. Li, H. Zhang, M. Jiang, Q. Zhang, P. He, X. Sun, 3D self-supported Fe-doped Ni_2P nanosheet arrays as bifunctional catalysts for overall water splitting, Adv. Funct. Mater. 27 (2017) 1702513.
[12] M. Gao, W. Sheng, Z. Zhuang, Q. Fang, S. Gu, J. Jiang, Y. Yan, Efficient water oxidation using nanostructured alpha-nickel-hydroxide as an electrocatalyst, J. Am. Chem. Soc. 136 (2014) 7077–7084.
[13] Y.P. Zhu, T.Y. Ma, M. Jaroniec, S.Z. Qiao, Self-templating synthesis of hollow Co_3O_4 microtube arrays for highly efficient water electrolysis, Angew. Chem., Int. Ed. 56 (2016) 1324–1328.
[14] X. Jia, Y. Zhao, G. Chen, L. Shang, R. Shi, X. Kang, G.I.N. Waterhouse, L.-Z. Wu, C.-H. Tung, T. Zhang, Ni_3FeN nanoparticles derived from ultrathin NiFe-layered double hydroxide nanosheets: an efficient overall water splitting electrocatalyst, Adv. Energy Mater. 6 (2016) 1502585.
[15] S.H. Gage, B.G. Trewyn, C.V. Ciobanu, S. Pylypenko, R.M. Richards, Synthetic advancements and catalytic applications of nickel nitride, Catal. Sci. Technol. 6 (2016) 4059–4076.
[16] Q. Zhang, Y. Wang, Y. Wang, A.M. Al-Enizi, A.A. Elzatahry, G. Zheng, Myriophyllum-like hierarchical TiN@Ni_3N nanowire arrays for bifunctional water splitting catalysts, J. Mater. Chem. A 4 (2016) 5713–5718.
[17] J. Huang, Y. Sun, Y. Zhang, G. Zou, C. Yan, S. Cong, T. Lei, X. Dai, J. Guo, R. Lu, Y. Li, J. Xiong, A new member of electrocatalysts based on nickel metaphosphate nanocrystals for efficient water oxidation, Adv. Mater. 30 (2018) 1705045.
[18] T. Liu, M. Li, C. Jiao, M. Hassan, X. Bo, M. Zhou, H.-L. Wang, Design and synthesis of integrally structured Ni_3N nanosheets/carbon microfibers/Ni_3N nanosheets for efficient full water splitting catalysis, J. Mater. Chem. A 5 (2017) 9377–9390.
[19] Y. Fan, S. Ida, A. Staykov, T. Akbay, H. Hagiwara, J. Matsuda, K. Kaneko, T. Ishihara, Ni-Fe nitride nanoplates on nitrogen-doped graphene as a synergistic catalyst for reversible oxygen evolution reaction and rechargeable Zn-air battery, Small 13 (2017) 1700099.
[20] Z. Cui, G. Fu, Y. Li, J.B. Goodenough, Ni_3FeN-supported Fe_3Pt intermetallic nanoalloy as a high-performance bifunctional catalyst for metal-air battery, Angew. Chem. 129 (2017) 10033.
[21] S. Nandi, S.K. Singh, D. Mullangi, R. Illathvalappil, L. George, C.P. Vinod, S. Kurungot, R. Vaidhyanathan, Low band gap benzimidazole COF supported Ni_3N as highly active OER catalyst, Adv. Energy Mater. 6 (2016) 1601189.
[22] M. Ledendecker, H. Schlott, M. Antonietti, B. Meyer, M. Shalom, Experimental and theoretical assessment of Ni-based binary compounds for the hydrogen evolution reaction, Adv. Energy Mater. 7 (2017) 1601735.
[23] B. Ouyang, Y. Zhang, Z. Zhang, H.J. Fan, R.S. Rawat, Nitrogen-plasma-activated hierarchical nickel nitride nanocorals for energy applications, Small 13 (2017) 1604265.
[24] W. Zhu, X. Yue, W. Zhang, S. Yu, Y. Zhang, J. Wang, J. Wang, Nickel sulfide microsphere film on Ni foam as an efficient bifunctional electrocatalyst for overall water splitting, Chem. Commun. 52 (2016) 1486–1489.
[25] X. Zhang, S. Zhang, J. Li, E. Wang, One-step synthesis of well-structured NiS–$Ni_2P_2S_6$ nanosheets on nickel foam for efficient overall water splitting, J. Mater. Chem. A 5 (2017) 22131–22136.
[26] J. Masud, S. Umapathi, N. Ashokaan, M. Nath, Iron phosphide nanoparticles as an efficient electrocatalyst for the OER in alkaline solution, J. Mater. Chem. A 52 (2016) 9750–9754.
[27] S.W. Kim, Y. Son, K. Choi, S.I. Kim, Y. Son, J. Park, J.H. Lee, J.H. Jang, Highly active bifunctional electrocatalysts for oxygen evolution and reduction in Zn-air batteries, ChemSusChem 11 (2018) 4203–4208.
[28] H. Yang, S. Luo, X. Li, S. Li, J. Jin, J. Ma, Controllable orientation-dependent crystal growth of high-index faceted dendritic $NiC_{0.2}$ nanosheets as high-performance bifunctional electrocatalysts for overall water splitting, J. Mater. Chem. A 4 (2016) 18499–18508.
[29] X. Kong, C. Zhang, S.Y. Hwang, Q. Chen, Z. Peng, Free-standing holey $Ni(OH)_2$ nanosheets with enhanced activity for water oxidation, Small 13 (2017) 1700334.
[30] C. Tang, N. Cheng, Z. Pu, W. Xing, X. Sun, NiSe nanowire film supported on nickel foam: an efficient and stable 3D bifunctional electrode for full water splitting, Angew. Chem., Int. Ed. 54 (2015) 9351–9355.
[31] C. Wu, P. Kopold, P.A. van Aken, J. Maier, Y. Yu, High performance graphene/Ni_2P hybrid anodes for lithium and sodium storage through 3D yolk-shell-like nanostructural design, Adv. Mater. 29 (2017) 1604015.
[32] W. Xi, G. Yan, Z. Lang, Y. Ma, H. Tan, H. Zhu, Y. Wang, Y. Li, Oxygen-doped nickel iron phosphide nanocube arrays grown on Ni foam for oxygen evolution electrocatalysis, Small 14 (2018) 1802204.
[33] J. Yang, F. Zhang, X. Wang, D. He, G. Wu, Q. Yang, X. Hong, Y. Wu, Y. Li, Porous

molybdenum phosphide nano-octahedrons derived from confined phosphorization in UIO-66 for efficient hydrogen evolution, Angew. Chem., Int. Ed. 55 (2016) 12854–12858.
[34] F. Hu, H. Yang, C. Wang, Y. Zhang, H. Lu, Q. Wang, Co-N-doped mesoporous carbon hollow spheres as highly efficient electrocatalysts for oxygen reduction reaction, Small 13 (2017) 1602507.
[35] T. Tang, W.J. Jiang, S. Niu, N. Liu, H. Luo, Y.Y. Chen, S.F. Jin, F. Gao, L.J. Wan, J.S. Hu, Electronic and morphological dual modulation of cobalt carbonate hydroxides by Mn doping toward highly efficient and stable bifunctional electrocatalysts for overall water splitting, J. Am. Chem. Soc. 24 (2017) 8320–8328.
[36] L. Hui, Y. Xue, D. Jia, H. Yu, C. Zhang, Y. Li, Multifunctional single-crystallized carbonate hydroxides as highly efficient electrocatalyst for full water splitting, Adv. Energy Mater. 8 (2018) 1800175.
[37] T. An, Y. Wang, J. Tang, W. Wei, X. Cui, A.M. Alenizi, L. Zhang, G. Zheng, Interlaced NiS_2–MoS_2 nanoflake-nanowires as efficient hydrogen evolution electrocatalysts in basic solutions, J. Mater. Chem. A 4 (2016) 13439–13443.
[38] C.C.L. McCrory, S. Jung, J.C. Peters, T.F. Jaramillo, Benchmarking heterogeneous electrocatalysts for the oxygen evolution reaction, J. Am. Chem. Soc. 135 (2013) 16977–16987.